Neoplasia 60 (2025) 101117

Contents lists available at ScienceDirect

Neoplasia

journal homepage: www.elsevier.com/locate/neo

Original Research

Galectin-3 secreted by triple-negative breast cancer cells regulates T cell function

Annat Raiter [a,b,c,*], Yael Barhum [a], Julia Lipovetsky [a,c], Chen Menachem [a,b], Sharona Elgavish [d], Shmuel Ruppo [d], Yehudit Birger [a,b,e], Shai Izraeli [a,b,e], Orna Steinberg-Shemer [a,b,e,1], Rinat Yerushalmi [a,b,c,f,1]

[a] Felsenstein Medical Research Center, Beilinson Campus, Petah Tikva, Israel
[b] Tel Aviv University, Faculty of Medicine and Health Sciences, Tel Aviv, Israel
[c] Rabin Medical Center, Beilinson Campus, Petah Tikva, Israel
[d] Bioinformatics Unit of the I-CORE, The Hebrew University of Jerusalem, Hadassah Ein-Karem campus, Medical School Building, Jerusalem, Israel
[e] The Rina Zaizov Hematology-Oncology Division, Schneider Children Medical Center of Israel, Beilinson Campus, Petah Tikva, Israel
[f] Davidoff Cancer Center, Beilinson Campus, Petah Tikva, Israel

ARTICLE INFO

Keywords:
Triple negative breast cancer
Galectin-3
T exhausted cells
Oxidative phosphorylation

ABSTRACT

Triple-negative breast cancer (TNBC) is an aggressive subtype that accounts for 10-15 % of breast cancer. Current treatment of high-risk early-stage TNBC includes neoadjuvant chemo-immune therapy. However, the substantial variation in immune response prompts an urgent need for new immune-targeting agents. This requires a comprehensive understanding of TNBC's tumor microenvironment. We recently demonstrated that Galectin-3 (Gal-3) binding protein/Gal-3 complex secreted by TNBC cells induces immunosuppression, through inhibiting CD45 signaling in T cells. Here, we further investigated the interaction between secreted Gal-3 and T cells in TNBC.

Using CRISPR/Cas9 gene editing of the TNBC MDA-MB-231 cell-line, we obtained Gal-3 negative$^{(neg)}$ clones. We studied these in an *in-vitro* model, co-cultured with peripheral blood mononuclear cells (PBMC) to imitate immune-tumor interaction, and in an *in-vivo* model, when implanted in mice.

Gal-3^{neg} tumors in mice had decelerated tumor growth after PBMC inoculation. In contrast, the Gal-3 positive$^{(pos)}$ tumors continued growing despite PBMC inoculation, and tumor T regulatory cell (CD4/FoxP3+) infiltration increased. RNA sequencing of T cells from women with TNBC with elevated plasma levels of Gal-3 revealed significantly lower expression of oxidative phosphorylation genes than in T cells from healthy women. Similarly, in our *in-vitro* model, the decreased expression of oxidative phosphorylation genes and mitochondrial dysfunction resulted in a significant increase in CD8 intracellular reactive oxygen species. Consequently, T exhausted cells (CD8/PD1/Tim3/Lag3+) significantly increased in PBMC co-cultured with Gal-3^{pos} TNBCs.

To conclude, we revealed a novel TNBC-related Gal-3 suppressor mechanism that involved upregulation of CD4 T regulatory and of CD8 T exhausted cells.

Introduction

Breast cancer is a highly heterogeneous disease that affects one in eight women worldwide[1]. Although great progress has been made in early detection and treatment, breast cancer remains the second cause of cancer-related mortality in women, after lung cancer[2]. Triple-negative

Abbreviations: Gal-3, Galectin-3; TNBC, Triple Negative Breast cancer; PBMC, Peripheral blood mononuclear cells; T-reg cells, T regulatory cells; ROS, Reactive oxygen species; rGal-3, Recombinant Gal-3; WT, Wild type; Gal-3^{neg}, Gal-3 mutated clones; Gal-3^{pos}, Gal-3 WT clones.

* Corresponding author at: Felsenstein Medical Research Center, Rabin Medical Center, Beilinson Campus, Petah Tikva, Israel.
E-mail addresses: araiter@tauex.tau.ac.il (A. Raiter), yael.barhum@gmail.com (Y. Barhum), juliali@clalit.org.il (J. Lipovetsky), chenmenahem@mail.tau.ac.il (C. Menachem), sharona.elgavish@mail.huji.ac.il (S. Elgavish), shmuel.ruppo@gmail.com (S. Ruppo), yehudit.birger@gmail.com (Y. Birger), sizraeli@gmail.com (S. Izraeli), orna.steinberg@gmail.com (O. Steinberg-Shemer), rinaty@clalit.org.il (R. Yerushalmi).

[1] Equal contribution

https://doi.org/10.1016/j.neo.2024.101117
Received 2 September 2024; Received in revised form 5 December 2024; Accepted 19 December 2024

breast cancer (TNBC), which accounts for 10-15 % of all breast cancer, is associated with the worse outcome [1,2]. Neoadjuvant chemo-immune therapy is the current clinical approach, aimed to prevent metastases in women with stage II and III TNBC. This regimen includes paclitaxel, carboplatin, anthracyclines and cyclophosphamide, in combination with pembrolizumab, an antibody targeting the immune checkpoint receptor programmed-cell death 1 (PD-1) [3]. Despite this protocol the prognosis is poor, prompting an urgent need for novel immune-targeting agents [4]. This requires comprehensive understanding of TNBC's molecular characteristics and tumor microenvironment including tumor immune interactions.

Galectin 3 (Gal-3) was described as an immune suppressor in various cancers. Overexpression of Gal-3 in tumor cells promotes its accumulation in the cytoplasm. Gal-3 is then transported to the cell surface and subsequently secreted to the extracellular space and circulation without a secretory signal sequence [5–10]. In the extracellular environment, Gal-3 intervenes in cell–cell and cell–matrix interactions and immunosuppression [11]. Galectin-3 has been shown to interact with cadherins and other cell surface glycoproteins, thereby influencing cell adhesion processes [11]. Additionally, it forms complexes with integrins and other proteins to activate signaling pathways that facilitate tumor cell adhesion to stromal cells [8]. Furthermore, Galectin-3 induces down-regulation of TCR/CD3 complexes in T cells following TCR engagement, leading to T-cell inactivation [12]. Elevated levels of Galectin-3 have been observed in both the plasma and tumors of women with TNBC, associated with poor prognosis [13]. We recently proposed a novel immunosuppressive mechanism, which may lead to new therapeutic approaches for non-responders to current therapeutic strategies. We showed that Gal-3 binding protein/tGal-3 complex is secreted by TNBC cells, and regulates immunosuppressive activity [14,15]. We further demonstrated that the Gal-3 complex increases the proportion of T regulatory cells (T-reg) in normal peripheral blood mononuclear cells (PBMCs) and induces increased secretion of the immunosuppressive cytokines IL- 10 and IL-35. We showed that the complex binds to the CD45 receptor on T cells and that it significantly increased interferon gamma (IFNγ) secretion and the percentage of CD4+/CD69+, CD8+/CD56+ and CD56+/CD69+ activated effector cells, which resulted in tumor cell killing [14,15].

In this study, we demonstrated additional contributions of secreted Gal-3 from TNBC cells to immunosuppression. We demonstrated that Gal-3 induces infiltrated T-reg in a TNBC in vivo model. For the first time, we revealed that Gal-3 induces a decrease in the genes involved in oxidative phosphorylation in T cells, which subsequently increases intracellular reactive oxygen species (ROS), leading to T cell exhaustion.

Material and methods

The cell line and cell cultures

We used MDA-MB-231 (obtained from ATCC, Biological Industries, Kibbutz Beit Ha Emek, Israel), a human TNBC cell line. Cells were grown in Dulbecco's Modified Eagle Medium (DMEM) supplemented with 10 % fetal calf serum (FCS), L-glutamine (2 mM), Na-pyruvate (1 nM), penicillin (100 μ/ml), streptomycin sulfate (0.1 mg/ml) and nystatin (12.5 μ/ml) (Biological Industries). Cultures were maintained at 37°C in a humidified 5 % CO_2 incubator. To maintain homogeneity and tumorigenicity of the cell line, a large stock of cells was prepared, and cells were used up to passage five. The cell line was examined for mycoplasma (mycoplasma detection kit, Biological Industries) at least once every six months.

PBMCs from healthy female volunteers and from TNBC patients were obtained from Magen David Adom National Blood Services or from Davidoff Cancer Center, Rabin Medical Center. The protocol was approved by the Institutional Review Board at Rabin Medical Center, Israel (0667-14-RMC). Samples were isolated by Ficoll–Hypaque density gradient (d = 1,077 g/mL, Ficoll-Paque Plus, GE Healthcare, Upsalla, Sweden) by centrifugation at 650 × g for 30 min. MDA-MB-231 cells derived from an exponentially growing monolayer were incubated overnight in 6-well plates at a concentration of 4×10^5/2 ml for each experiment. PBMCs were cultured in complete RPMI medium, supplemented with 5 % AB serum (Gibco, Brasil), and were added on to the tumor cells (2×10^6/ml). Recombinant Gal-3 (rGal-3) protein at 2μg/ml (R&D Systems, USA) was added to the Gal-3^{neg} clones.

T cell isolation from PBMCs

T cells were isolated by negative selection using the Pan T isolation kit (Miltenyi Biotec, USA) following the manufacturer's instructions. After separation, >90 % of the cells were identified as CD3+ by flow cytometry analysis.

CRISPR/Cas9 genome editing of Gal-3

Gal-3^{neg} cells were generated by the CRISPR/Cas9 gene editing method. The guide was designed by the "GoGenome" software generated by the CRISPR-IL consortium. The guide sequence: CATGGTTTGAAGCATCCACA GGG targets ch14:55133375. To genetically edit MDA-MB-231 cells, we used the ribonucleoprotein system (the Alt-R® CRISPR-Cas9 System, IDT) and the 4D electroporation system (Lonza, Basel, Switzerland) with the SE buffer and program CH125. Forty-eight hours after electroporation we harvested the cells and extracted DNA to analyze editing by next generation sequencing (NGS). Polymerase chain reaction (PCR) was performed to amplify the edited region using the following primers: Forward 5` -GGGCCACCATGTTATCTCTCTG-3` and Reverse: 5`-GTACTGTCCTGCCATCTCACTG-3`. A second PCR was done with Illumina barcode primers. Barcoded PCR was analyzed by NGS (Illumina) and the results were analyzed in the CRISPRESSO2 software. The cells were diluted to single cells per well, to generate genetically homogenous sub-clones. DNA was extracted from each clone PCR product, sent to Sanger analysis and detected with ICE software (Syntego). Guide specificity was studied by GuideSeq analysis (performed by HYLABS). Predicted changed loci in the genome were further amplified and studied by NGS with specific primers (Supplementary Table 1).

Gal-3 mRNA expression

Gal-3 RNA expression was studied by real time (RT)-PCR. mRNA was isolated with Trizol (Invitrogen, Thermo Fisher Scientific, USA) and cDNA was prepared. cDNA was detected using the primers: Forward 5`-GCGTTATCTGGGTCTGGAAACC-3` and Reverse: 5`-GCACTTGGCTGTCCAGAAGATG-3` at 60°C annealing temperature and analyzed by RT-PCR.

Gal-3 cell surface protein expression was evaluated by flow cytometry analysis using anti-Gal-3-PE, 0.125μg/0.5 × 10^6 cells (R&D Systems). Cells were trypsinized, and 0.5 × 10^6 cells/50 μl of phosphate buffered saline (PBS) were incubated with the anti-Gal-3 antibody for 30 min at room temperature. Cells were washed and gated live cells were analyzed using the Coulter Navious FACS and the Kaluza software.

For total Gal-3 protein expression studies, we used Western blot. Cells (1×10^6) were re-suspended in 0.12 ml of lysis buffer (20 mM Tris-HCl pH 7.5, 150 mM NaCl, 1 mM NaF, 2 mM Na_3VO_4, 1 % NP40, 10 mM b-glycerophosphate, 30 % glycerol, 1 mM EDTA,0.5 % sodium-deoxycholate, 0.5 % protease inhibitor cocktail), followed by one freeze-thaw cycle of 20 min. Cells were harvested and centrifuged (14,000 rpm, 15 min, 4°C). Supernatants were collected, and aliquots were separated on 10 % SDS PAGE, followed by Western blotting with anti-Gal-3 biotinylated 0.1μg/ml (R&D Systems, USA). The secondary antibody, IRDye 800CW Goat anti-Rabbit or IRDye 680CW Goat anti-Mouse (1mg/ml, LI-COR, Nebraska, USA) was added for 1h. Secreted Gal-3 was evaluated by a method developed in our laboratory and previously published [15].

Colony formation

Spheroid formation was performed following Yamaguchi et al. [16]. In brief, dissociated MDA-MB-231 monolayers (Passage 3) were resuspended in medium to obtain a single cell suspension. TNBC cells (5×10^4 cells/well) were added to Nunc®Low Cell Binding Surface 96-well plates (Thermo Scientific Nunc A/S, Denmark) and incubated in DMEM medium supplemented with FBS and penicillin-streptomycin at 37°C for up to 7 days.

Cell proliferation

MDA-MB-231 cells (1000 cells/well) or PBMCs (40,000 cells/well) were seeded on 96 wells in triplicates, and proliferation was measured using the Cell Proliferation Kit (Sartorius, USA) following manufacture instructions, after 1 day or 3 days, respectively.

Tumor xenograft growth in mice

The animal experimental procedures used in this study were approved by the Animal Care and Use Committee of Tel Aviv University (TAU 06-01-20220) and performed according to their guidelines. Tumor xenografts were generated by subcutaneously injecting 4×10^6 wild type (WT) MDA-MB-231(Gal-3^{pos}) cells, or 4×10^6 Gal-3 mutated (Gal-3^{neg}) cells into the right flank of NOD/SCID/gamma-chain knockout (NSG) female mice (7-8 weeks of age; each weighing 18-22 g). Mice were randomized to two groups (8-10 mice/group): Gal-3^{pos} cells and Gal-3^{neg} cells. Tumor volumes were measured every other day using micrometer calipers and were calculated according to the following formula: tumor volume (mm^3) = 0.5 x D x d^2, where d and D represent the shortest and the longest diameters, respectively. One week after tumor injection, when the xenograft grew to approximately 30 mm^3, fresh human PBMCs from two female donors were inoculated by an intravenous injection, into half of the mice for each donor. At the end of the experiment (23 days after the administration of the PBMCs), the mice were bled for the measurement of human IL-35 in serum and sacrificed for the extraction of tumors (Fig. 3A).

Immunofluorescent staining

Tumor tissues underwent 4 % formalin fixation overnight at 4°C and paraffin embedding. The specimens were then sliced into 5-μm-thick sections, and deparaffinized in xylene and rehydrated in alcohol. After antigen retrieval at pH=6 and washing with deuterium depleted water (DDW), the sections were blocked in bovine serum albumin (BSA) 3 % (Bioworld, Canada) and 10 % Triton-X100 (Merck KGaA, Germany) for 10 min. After washing with PBS, the slides were incubated for 1 h with primary antibodies: CD3-APC (1:50, Beckman Coulter, France), FOXP3-FITC (0.1 μg, R&D systems) and Gal-3-PE (1:25, R&D systems), HLA-A (Rabbit Monoclonal, cat#Ab52922, 1:100, Abcam, followed by Alexa Fluor 488 AffiniPure Donkey anti Rabbit IgG, 1:200 from Jackson Immunoresearch Laboratories, USA). Slides stained with an IgG irrelevant antibody and secondary antibodies served as negative controls. Human-derived PBMC paraffin slides served as positive controls. DAPI (4′,6-Diamidino-2-P henylindole, Dilactate) (cat#BLG-422801, 1:400, Biolegend, USA) was used as counterstain. Fluorescence was observed and images acquired using a Leica TCS SP5 confocal laser-scanning microscope (Leica Microsystems, Germany). Quantitative image analysis was performed using FIJI (Image J2) analysis software in five fields/slide in five distinct slides.

Flow cytometry analysis for identifying activated and suppressed immune cells

PBMCs (2×10^6/ml) were seeded on Gal-$3^{neg/pos}$ cells and rGal-3 was added for 3 or 5 days. Then, PBMCs were extracted from the co-cultures, centrifuged and resuspended in PBS (5 % FBS (Gibco, Brasil) and 1 % Na Azide, SIGMA Aldrich, USA) for flow cytometry analysis. To assess T-reg, PBMCs (0.5×10^6/50 μl PBS) were incubated with the following antibodies for multicolor staining, for 40 min at room temperature: CD4-PC7, CD8-KO, CD25-APC-AF 750 and CD69-PC-5 (Beckman Coulter,). For FOXP3 intracellular staining, cells were treated with permeabilization buffer (R&D Systems). Cells were then washed twice for 10 min (1200 rpm, 4°C).

To assess T exhausted cells, the following antibodies were used: CD8-KO, (Beckman Coulter), PD1-AF647, LAG3-AF700 and TIM3-AF405 (R&D System, USA). To assess intracellular ROS, the Cellular ROS-FITC Assay kit (Abcam, cat Number: ab113851, USA) was used.

RNA sequencing

RNA was isolated from PBMCs of four healthy female donors and of four women diagnosed with TNBC stage 4, using RNeasy Plus mini-Kit (Qiagen). All the samples were procured according to the protocol approved by the Institutional Review Board of the Rabin Medical Center (0667–14-RMC).

Bulk RNA-seq analysis**:** raw reads were quality-trimmed, and the remaining adapter sequences were removed using cutadapt (v2.10) [17]. Processed reads were aligned to the human genome version GRCh38 (with genome annotations of Ensembl release 99) using TopHat (v0.11.9) [18]. Quantification was done with htseq-count (v0.6.0) [19], with strand information set to 'reverse'. Differentially expressed genes were identified using DESeq2 (v1.26.0) [20]. Pair-wise comparisons were tested with default parameters, except for omitting the independent filtering algorithm. The significance threshold was set to padj<0.1 (default).

RNA-Seq counts were converted to TPM, the recommended unit for deconvolution analysis [21]. This was performed using CIBERSORTx, a machine learning method that enables estimating cell type abundances from bulk tissue transcriptomes and calculating cell-type-specific gene expression profiles [22]. The ABIS RNA-seq signature matrix [23], which has demonstrated a T-cell fraction of 50-70 %, was employed rather than LM22, CIBERSORTx's signature matrix. The latter indicated overestimation of the monocyte fraction (30-40 % instead of the expected 10-20 %). The RNA-Seq raw counts were converted to TPM using the convertCounts function from R DGEobj.utils package (with normalize=none, and log=FALSE parameters). The length per gene was defined as the length of merged exons of the gene's isoforms, calculated with GTFtools [24]. GRCh38 genome and Ensembl 99 annotations were used. From the initial pool of 26,094 genes, those with low expression and zero variance were filtered out. DEGs of the T-cell gene expression profile of PBMCs of women with TNBC vs those of healthy women were identified using the limma package [25]. TPMs were log2-transformed, and gene-level variance was modeled using the limma-trend. Non--cutoff-off dependent downstream analysis was conducted by performing Gene Set Enrichment Analysis (GSEA) [26] using the GENI web-based platform [26]. The genes that were used in this analysis were ranked by a metric of multiplication of -log10(Pval), with −1/1 for the upregulated and downregulated genes, respectively.

Oxidative phosphorylation gene expression

We isolated T cells from PBMCs of healthy donors and from women with TNBC before treatment. Then, we used a co-culture TNBC model consisting of PBMCs incubated with Gal-3^{pos} or Gal-3^{neg} clones, with or without rGal-3. We extracted RNA from the isolated T cells as described above.

RNA quantity and quality were determined by OD at 260 and 280 nm using nanoDrop 1 (Thermo Scientific, USA). RNA was converted to cDNA using the High-Capacity RNA to cDNA kit (Thermo Fisher Scientific). The SYBR green system (Applied Biosystems, Thermo Fisher Scientific., USA) was used to target genes. Fluorescent accumulation was

analyzed by StepOnePlus RT-PCR (Applied Biosystems, Thermo Fisher Scientific, USA). G0ene expression was normalized to GAPDH. The primer pairs from Hy Laboratories LTD, (Israel) are listed in Supplementary Table 2.

Cytokine secretion

IL-10 concentrations were determined with ELISA Ready SET-Go (eBioscience, Thermo Fisher Scientifics, USA) according to the manufacturer's instructions. Human IL-35 was determined with ELISA using kits from Elabscience Biotechnology following the manufacturer's instructions.

Statistical analysis

All experiments were independently replicated at least three times. Statistical analyses were performed using GraphPad Prism 2024 software. Results are presented as mean ± standard deviation (SD) or standard error (SE), as appropriate. A two-tailed Student's t-test was used for experiments with a single outcome, and one-way ANOVA was applied for comparisons involving multiple groups. A p-value of <0.05 was considered statistically significant.

Results

Gal-3 knocked-out in the MDA-MB-231 TNBC cells

To determine the effects of Gal-3, we knocked-out Gal-3 in MDA-MB-231 TNBC cells using the CRISPR/Cas9 genome editing method. A designed guide located in exon 1 of Gal-3 with Cas9 protein efficiency cut the Gal-3 gene (89.56 %). Deletion of one nucleotide was apparent in 37 % of the bulk-edited cells (Supplementary Fig.1). As a result of CRISPR editing, the isolated clone 1 is a compound heterozygous for two variants, including a single nucleotide deletion and a single nucleotide insertion, both leading to frameshift. Clones 2 and 3 are homozygous for a single nucleotide frameshift variant. The WT Gal-3^{pos} clone was isolated from edited cells in which Gal-3 was uncut (Fig. 1A). Off-target analysis revealed a mutation in the *ITGA10* gene (Supplementary Fig. 2). However, this mutation was found in all the clones, including the Gal-3^{pos} control. RT-PCR revealed significantly lower Gal-3 mRNA expression (Fig. 1B). Western blot and flow cytometry analysis revealed cell surface and total protein downregulation in the negative clones (Fig. 1C and D respectively). We observed significantly lower expression of Gal-3 total protein (3-fold, $p = 0.02$, Fig. 1C). Cell surface protein expression was significantly lower, by 6-fold ($p = 1.9 \times 10^{-6}$). In the Gal-3^{neg}, the overall protein expression was significantly lower than in the Gal-3^{pos} clones. Whereas Gal-3 mRNA was lower in only 50 %, Gal-3 secretion was lower by 2-fold in the Gal-3^{neg} clones (Fig. 1E) ($p = 2.3 \times 10^{-9}$). In agreement, the concentration of Gal-3 was lower in the plasma of healthy women than of TNBC patients (Fig. 1F), although large variability was noted within the groups.

Gal-3 affects tumor cell and leukocyte proliferation

To assess whether Gal-3 affects tumor cell proliferation, we compared the proliferative capacity of the mutated and the Gal-3^{pos} clones. In 10 repeated experiments, we observed significantly lower proliferation of the Gal-3^{neg} clones (1.6-fold lower, $p = 0.000001$, Fig. 2A). This result correlated with the capacity of cells to form 3D spheroids. The capacity was significantly lower for the Gal-3^{neg} than the

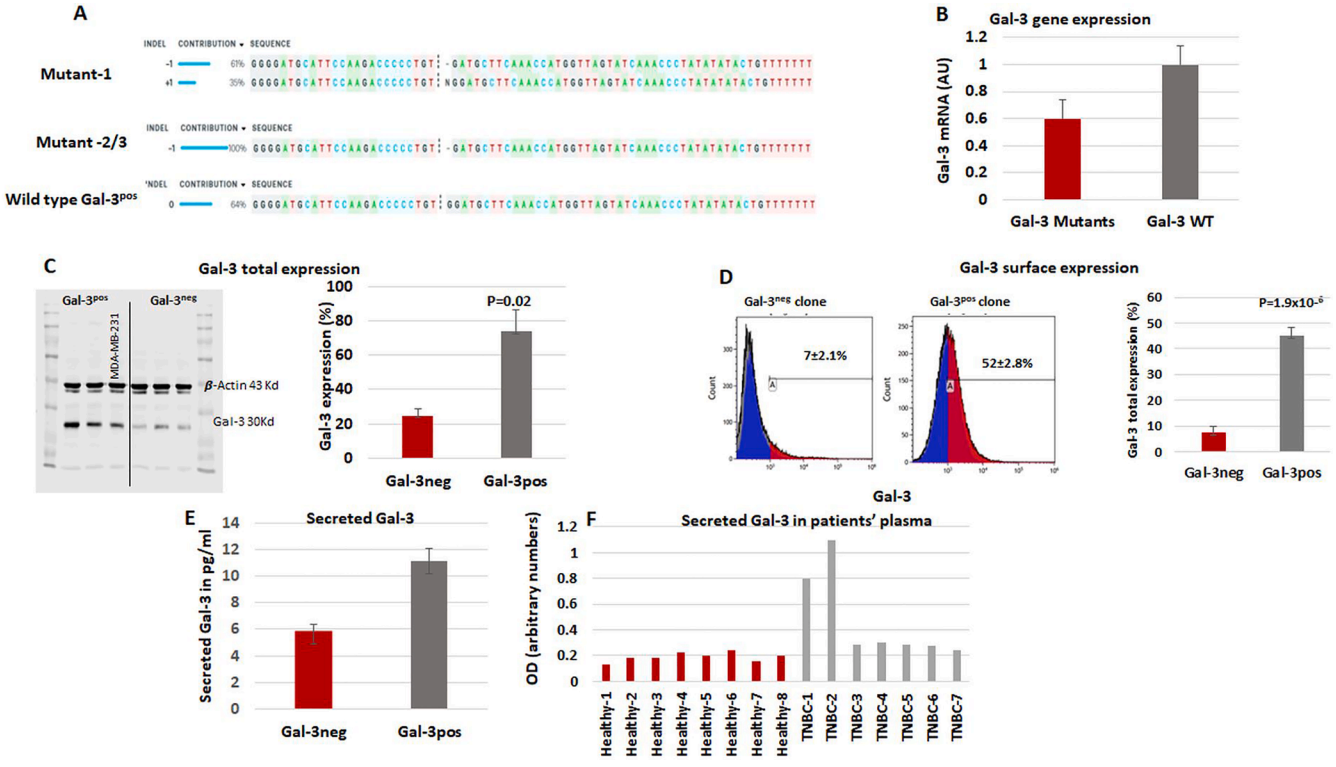

Figure 1. Gal-3 expression.
A. Sequencing analysis of three edited clones (ICE sofware). **B.** Gal-3 mRNA expression studied by RT-PCR, showing less Gal-3 mRNA in the Gal-3^{neg} than the Gal-3^{pos} clones. **C.** SDS-Page gel showing total expression of the Gal-3 protein in three mutated clones (Gal-3^{neg}) compared to unedited MDA-MB-231 and two Gal-3^{pos} clones evaluated by Western blot. The bar graph compares the mean±SD of the Gal-3^{neg} and the Gal-3^{pos} clones. **D.** A representative histogram showing Gal-3 cell surface expression measured by flow cytometry analysis. In red, Gal-3^{pos} expression. The bar graph shows the mean±SD Gal-3 total expression of the Gal-3^{neg} clones and the Gal-3^{pos} clones. **E.** The mean±SD of the secreted Gal-3 protein by the mutated and the Gal-3^{pos} clones, evaluated by ELISA. **F.** Optical density (OD) of secreted Gal-3 in the plasma of seven healthy women and six women with TNBC, measured by ELISA.

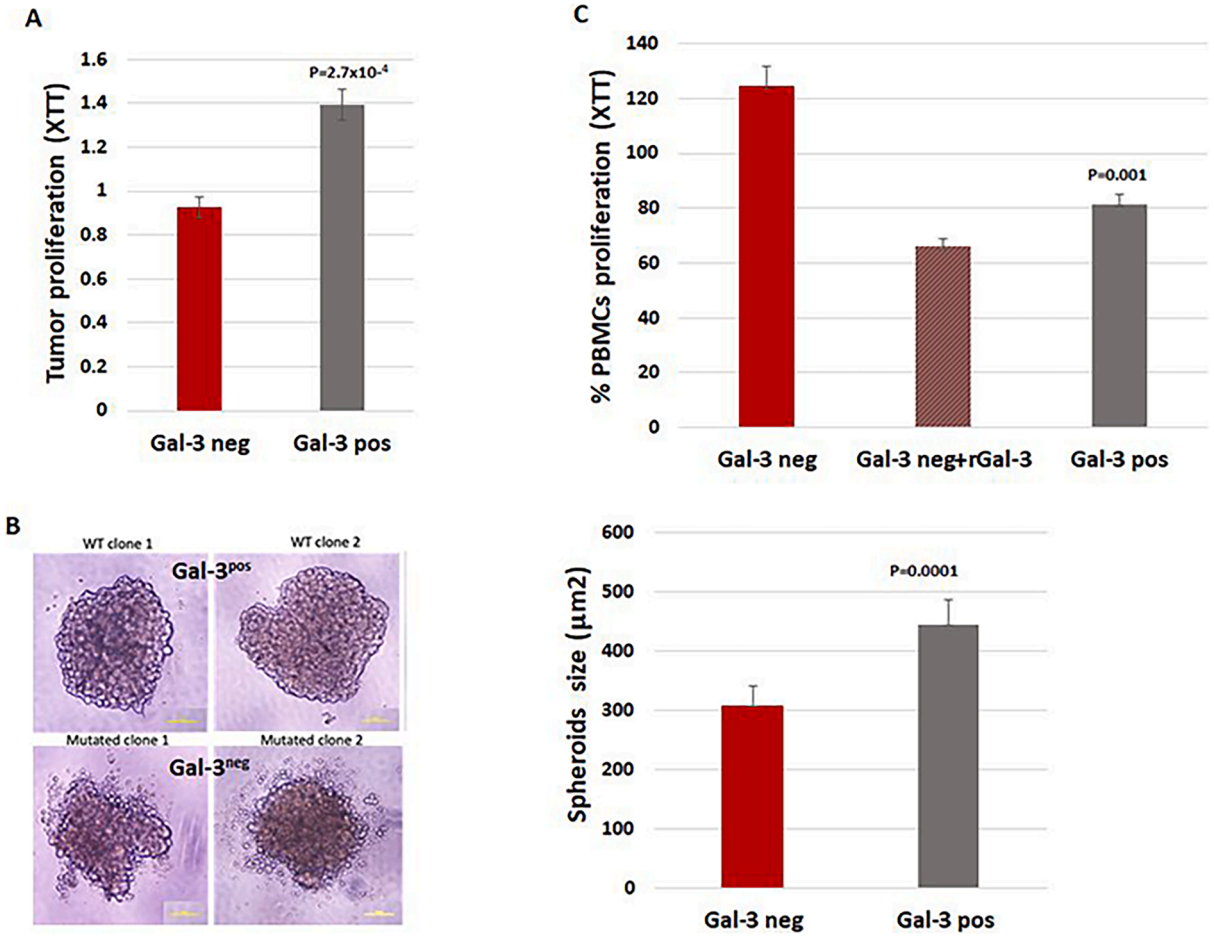

Figure 2. The effect of Gal-3 on cell proliferation.
A.Tumor cell proliferation evaluated by XTT assay. Mean±SD values are presented for Gal-3^{neg} vs Gal-3^{pos} ($n = 10$). **B**. A representative picture (light microscope, scale bar=100µ m, showing spheroid formation by Gal-3^{neg} and Gal-3^{pos} clones. On the right, a quantitative analysis of spheroid size, compares Gal-3^{neg} to Gal-3^{pos} clones. The bar graph shows mean±SD in µm^2 of 3D spheroids ($n = 3$). **C.** The bar graph shows peripheral blood mononuclear cell (PBMC) proliferation following culturing with supernatants of Gal-3^{neg}, Gal-3^{neg} + rGal-3, and WT clones. Bar graph, mean±SD, $n = 5$.

Gal-3^{pos} clones (1.44-fold less, $p = 0.0001$, Fig. 2B).

Subsequentially, we evaluated the effect of Gal-3 on PBMC proliferation. For this, PBMCs from healthy women were incubated with supernatants generated from cultures of Gal-3^{neg} clones, with and without the addition of rGal-3, and with supernatants of WT clones (Fig. 2C). The mean PBMC proliferation was significantly lower following the addition of rGal-3 to supernatants of Gal-3^{neg} clones (1.9-fold less, PBMCs from five volunteers, $p = 0.001$). These results correlated with 1.5-fold lower PBMC proliferation when cultured with supernatants of WT clones ($n = 10$, $p = 0.003$).

Gal-3 impacts tumor growth and increases infiltrated T-reg in vivo

To confirm the tumor cell anti-proliferative effect of Gal-3, we performed an *in vivo* experiment. Mice were subcutaneously inoculated with Gal-3^{neg} or Gal-3^{pos} clones. Human PBMCs from healthy women were intravenously injected one week after tumor engraftment (Fig. 3A).

As observed for cell proliferative capacity *in vitro*, the growth rate of tumor cells from the Gal-3^{neg} clones was lower than that of the Gal-3^{pos} cells ($p > 0.05$ at all time-points). Nevertheless, during the first 10 days, the mutated cells maintained a steady rate. However, one week after PBMC inoculation, reduced cell growth was detected (Fig. 3B). We hypothesized that this deceleration in tumor growth indicated involvement of Gal-3 on human leukocytes. To further examine this, we first validated the expression of Gal-3 in the tumor (in red), and found it under expressed in mutant clones (Fig. 3C, a representative mouse biopsy stained with anti-human HLA-A antibody (green) to identify the human tumor cells engrafted in mice).

We subsequently detected a direct correlation between the number of T-reg infiltrated cells (CD3+FOXP3+) and CD3+ cells in the same samples (Fig. 3D). Though the numbers of CD3^{pos} cells were similar in the two groups, the number of T-reg was greater in the biopsies of Gal-3^{pos} than Gal-3^{neg} cells ($p = 0.004$, Fig. 3E). The increase in T-reg in the WT cells correlated with a greater increase of IL-35 in the serum of mice injected with Gal-3^{pos} cells than with mutated cells ($p = 0.006$, Fig. 3F).

Secreted Gal-3 induced an increase in T-reg

To further examine the effect of Gal-3 on T-reg, we performed an *in vitro* experiment. After adding r-Gal-3 to co-cultures of PBMCs, T-reg was 2.5-fold greater in those with Gal-3 ^{neg} clones ($p = 0.0007$, Fig. 4A). Similarly, for PBMCs incubated with Gal-3^{pos} clones, T-reg was 1.9-fold greater than in the Gal-3^{neg} clones ($p = 0.031$ vs mutants). The proportion of T-reg did not differ significantly between PBMCs incubated with Gal-3^{neg} treated with rGal-3 and Gal-3^{pos} cells. These results correlate with the significant increase in IL-35 in supernatants of PBMCs cultured with Gal-3^{neg} clones with the addition of r-Gal-3 ($p = 0.034$, Fig. 4B), or PBMCs cultured with Gal-3^{pos} clones ($p = 0.001$, Fig. 4C). A significant increase was also observed in IL-10 in the same supernatants of the co-cultures ($p > 0.05$ for both vs Gal-3^{neg}). In contrast, the

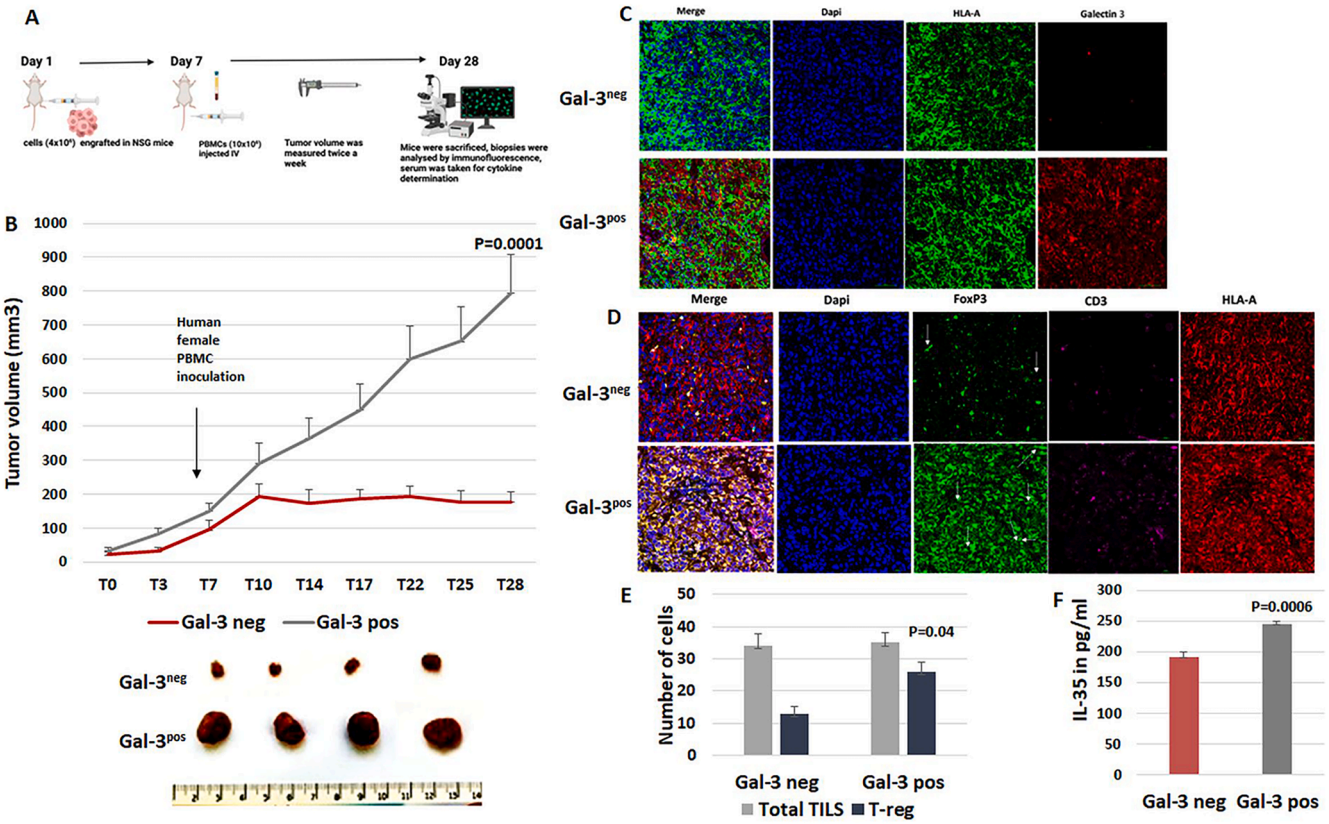

Figure 3. The effect of Gal-3 on tumor growth and infiltrated T reg cells in vivo.
A. The scheme of the mice experiment protocol. **B**. Tumor volume is compared following the injection of Gal-3^{neg} vs. Gal-3^{pos} (mean±SE of 8-10 mice in each group, significance was calculated by the T-test). PBMCs of healthy women were intravenously inoculated one week after tumor injection. Below, four samples per group of gross tumor images. **C.** Confocal microscope immunofluorescent staining images of the expression of Gal-3 in Gal-3^{pos} and Gal-3^{neg}. In green, HLA-A was used to identify human tumor cells. In red, Gal-3. Dapi (blue) was used for nucleai staining. Scale bar=20μm. **D.** Confocal microscope immunofluorescent staining images of T-reg. Human HLA-*A*+ tumor cells are in red. CD3, used to identify T cells, are in purple. In green is FOXP3 staining. In yellow are T-reg and tumor cells that express FOXP3 and CD3. The scale bar=20μm. Arrows show T-reg cells in both groups. **E**. The bar graph shows mean±SE of CD3/FOXP3 positive cells in three slides of four mice injected with Gal-3^{pos} clones compared to Gal-3^{neg} clones (mean±SE, significance calculated by the T-test). **F.** IL-35 concentration (pg/ml) in the serum of six mice in each group (mean±SE, the significance was calculated by the T-test).

proportion of activated cells (CD4^{+}/CD69^{+}) was lower following the addition of r-Gal-3 to the Gal-3^{neg} clones, as well as in the PBMCs incubated with the Gal-3^{pos} clones (Fig. 4D). Anti Gal-3 antibody decreased the percentage of T reg cells in Gal-3 pos co-cultures (Supplementary Fig. 3).

T cells from TNBC patients showed significantly lesser oxidative phosphorylation gene expression

To reveal immune dysregulation relevant to women with TNBC, we performed RNA seq of PBMCs collected from women with TNBC and from healthy women. Downstream analysis of 1460 differentially expressed genes (DEGs, Padj<0.1) revealed enriched pathways involving myeloid cell lines, even though PBMCs typically comprise 70–90 % lymphocytes (data not shown). This finding suggests variation in PBMC purification among the samples, possibly related to technical variations at a number of steps.

To address this variability, data deconvolution was performed to isolate a T-cell gene expression profile from RNA-Seq results. T-cells were selected due to their accuracy of deconvolution calculations for cell populations comprising a significant percentage of the total cell population [27]. GSEA of the PBMC T-cell gene expression profiles showed that the oxidative phosphorylation (MSigDB hallmark) gene set was significantly enriched in the down-regulated genes in the TNBC patients compared to the healthy women (false discovery rate <0.05) (Fig. 5A and B, before and after deconvolution, respectively). The downregulation of MDH2, SUPV3L1, GOT2 and GPI genes highly contributed to the enrichment of downregulated genes in the oxidative phosphorylation (MSigDB hallmark) of the women with TNBC compared to the healthy women (Fig. 5C).

To validate the results obtained by the bioinformatic analysis, we selected the five genes with the highest statistical differences, from all the genes that were involved in oxidative phosphorylation and down-regulated in women with TNBC. T cells were isolated from co-cultures of PBMCs, with the different clones, to evaluate gene expression. We compared the gene expression of T cells isolated from six women with TNBC vs T cells from healthy women (Fig. 5D). We observed lesser gene expression of SLC25A6 (34 %), MDH2 (43 %), GPI (54 %) and GOT2 (80 %). Only for SUPV3L1 was the expression greater, by 50 %. Similarly, the expression levels of all the genes in T cells isolated from the co-cultures were lower for those with Gal-3^{pos} than with Gal-3^{neg} clones (Fig. 5E). T cells from the Gal-3^{pos} co-cultures showed lower expression of SLC25A6 in 46 % ($p = 0.00005$), lower MDH2 expression in 29 % ($p = 0.007$), lower SUPV3L1 in 23 % ($p = 0.01$) and lower GOT2 in 59 % ($p = 0.002$). GPI expression was lower but not significantly ($p = 0.1$), probably due to its genetic variants [28].

Gal-3 induced intracellular ROS and an increase in T cell exhausted cells

Mitochondrial dysfunction is characterized by decreased expression of genes related to oxidative phosphorylation [29] and can lead to increased intracellular ROS [30]. We observed a 2.6-fold higher

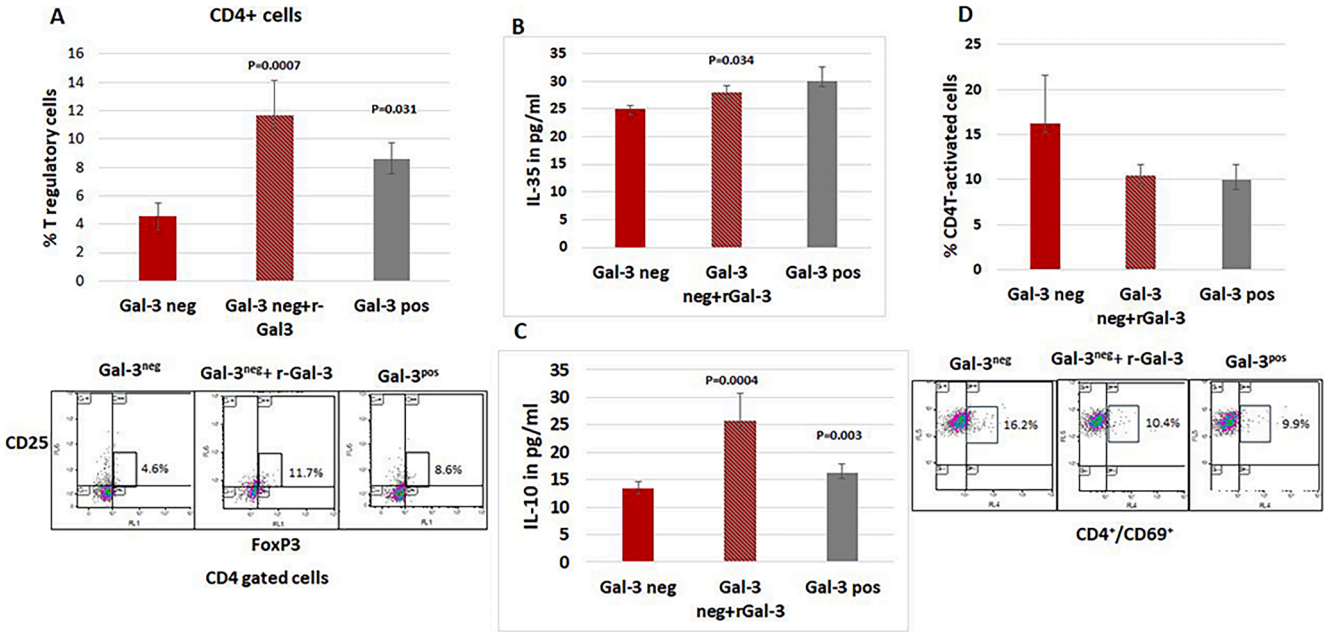

Figure 4. The effect of Gal-3 on T reg cells in vitro.
A. The percentage of T-reg cells in co-cultures of PBMCs with Gal-3^{neg} ± *r*-Gal-3 or with Gal-3^{pos} clones after 3 days incubation. Mean±SE, $n = 10$, the significance was calculated by ANOVA. Below, a representative flow cytometry study shows CD4 gated cells, positive for CD25 and FOXP3. **B** and **C.** Assessments of IL-35 and IL-10 in supernatants of the same co-cultures. **d.** The percentage of activated CD4+/CD69+ cells obtained from co-cultures of PBMCs with Gal-3^{neg} ± *r*-Gal-3, or with Gal-3^{pos} clones. Mean±SE, $n = 5$. Below, a representative flow cytometry analysis showing a lower percentage of activated CD4+ cells after Gal-3 compared to the other cultures.

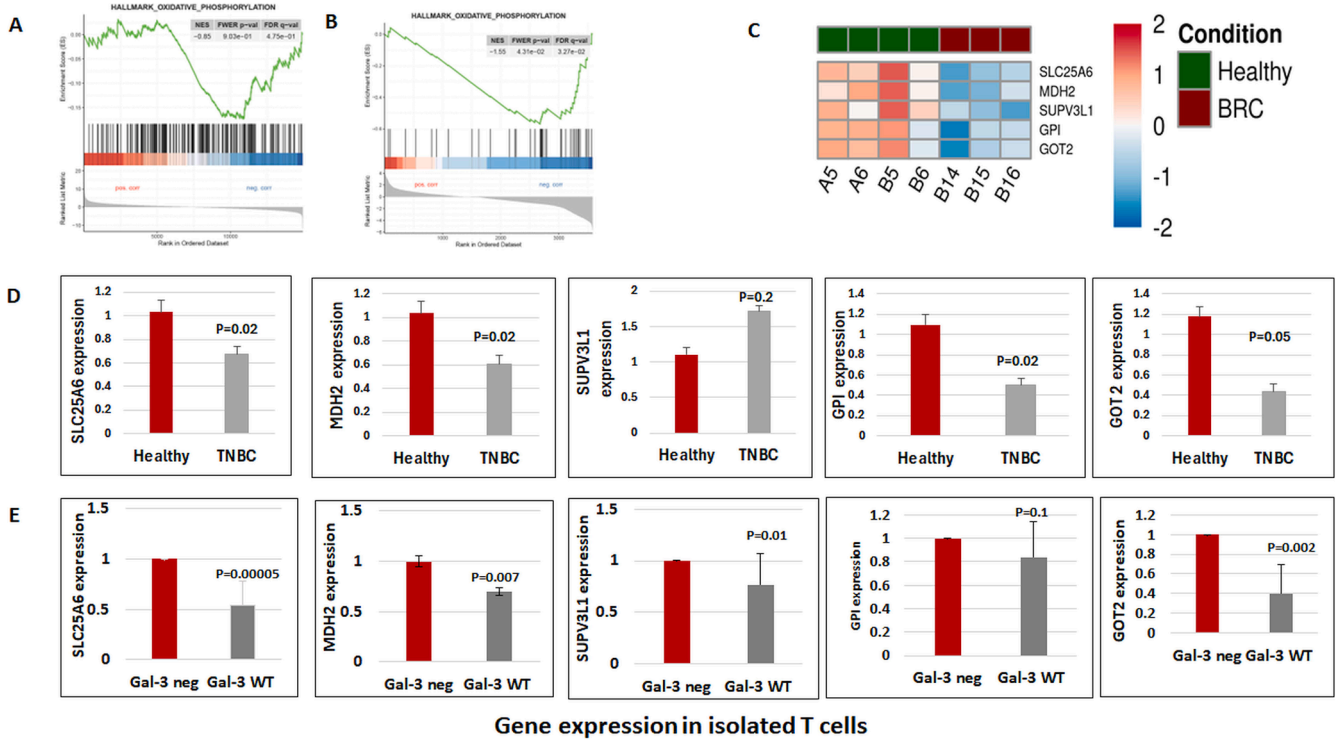

Figure 5. The effect of Gal-3 on oxidative phosphorylation genes.
A. Gene Set Enrichment Analysis of transcriptome data of PBMCs of women with TNBC and healthy controls, in bulk RNA-Seq before deconvolution. **B.** T-cell transcriptomic gene expression after deconvolution. The oxidative phosphorylation hallmark MSigDB gene set is significantly enriched in the downregulated genes of the T-cell transcriptome, but not in the bulk transcriptome. **C.** Heatmap of the expression of five selected genes from PBMCs of four women with TNBC and four healthy female volunteers. **D.** Validation of gene expression in isolated T cells from PBMCs of six patients compared to six healthy donors. Mean±SD and significance were calculated by the T-test. **E.** Oxidative phosphorylation gene expression in T cells isolated from PBMCs co-cultured with Gal-3^{neg} compared to Gal-3^{pos} clones. Mean±SE, $n = 6$. The signifcance in each of the five genes is calculated by the T-test.

intracellular ROS in CD8 cells isolated from co-cultures of Gal-3^{neg} clones treated with rGal-3 vs PBMCs incubated with Gal-3^{neg} ($p = 0.03$, Fig. 6A). Similarly, CD8 T cells isolated from co-cultures with Gal-3^{pos} clones showed 2.3-fold higher intracellular ROS compared to mutants ($p = 0.03$). No statistical difference was noted following the addition of rGal-3 to the Gal-3^{neg} or to the Gal-3^{pos} co-cultures. We also observed a greater proportion of T cell exhausted cells, marked by PD-1, TIM-3, and Lag-3 expression. The addition of rGal-3 induced a 1.9-fold increase in T exhausted cells ($p = 0.04$) after 5 days in culture (Fig. 6B). A similar increase in exhausted T cells was noted in T cells isolated from co-cultures with Gal-3^{pos} cells (1.6-fold increase, $p = 0.011$). After 3 days of incubation, no significant differences in intracellular ROS and exhausted T cells were detected between the 3 groups (Supplementary Fig. 4A, B).

Discussion

In this study we describe novel immunosupressive functions of Gal-3 secreted from TNBCs, which impacted both CD4 and CD8 cells. To examine the immunosuppresive mechanisms of Gal-3, we generated Gal-3^{neg} clones in MDA-MB-231 TNBC cells, and assembled *in vitro* and *in vivo* models.

We found significantly higher levels of Gal-3 in the plasma of women with TNBC than in healthy women. Of note, the TNBC blood samples demonstrated variable Gal-3 levels, which may be due to the heterogeneity of the disease [31]. To reproduce the heterogeneity of TNBC pathology, we used our in vitro model, which consisted of co-culture of PBMCs from healthy women with either Gal-3^{pos} or Gal-3^{neg} clones [32,33]. Gal-3 extracellular and plasma levels in TNBC patients are known to correlate with chemotherapy efficacy. Increased Gal-3 secretion due to chemotherapy was related to better prognosis and longer disease-free survival [34]. In contrast, another study revealed that a high Gal-3 concentration in the plasma of TNBC patients was associated with greater tumor size, particularly in those who did not respond to chemotherapy [35]. Higher Gal-3 levels were also reported in TNBC compared with other breast cancer subtypes and were related to its poor prognosis [13]. This was attributed to a protective role of Gal-3 in human breast cancer cells against tumor necrosis factor α and nitric oxide-induced apoptosis [36].

Our first approach was to examine the effect of extracellular Gal-3 on TNBC cells. We demonstrated that Gal-3 induced tumor growth and 3D spheroid formation. In the spheroid formation and the *in-vivo* study, we observed that cells did not lose their capacity to replicate, but growth rate acceleration was noted in the presence of Gal-3. In contrast, previous studies using MDA-MB-435 melanoma cells, showed down-regulation of Gal-3 expression, which resulted in reduced tumor growth *in vivo* [37,38].

In our *in vivo* model, tumor growth started to decelerate six days after human PBMC transplantation in mice injected with Gal-3 mutated clones. This development was evidently linked to the immunosuppressive role of Gal-3 [15,39]. Gal-3 binds carbohydrate ligands in cell membrane glycoprotein receptors like CD45, and the T cell receptor. This alters the spatial organization of the immune synapses, and results in the suppression of T cell activation [14,39,40]. We found that over-expression of Gal-3 correlated with higher numbers of infiltrated T-reg and with higher levels of IL-35 in the serum of mice inoculated with Gal-3^{pos} tumors. This is probably due to the binding of extracellular Gal-3 to CD45 on T cells [15]. These results were validated *in vitro* by the addition of rGal-3 to co-cultures of PBMCs with Gal-3^{neg} clones, which resulted in higher numbers of T-reg and of interleukins 10 and 35 in co-culture supernatants. Recent studies highlight the role of tumor-infiltrating macrophages (TAMs) as a negative prognostic factor in breast cancer, aligning with their significant involvement in the tumor microenvironment [41]. Effect of Gal-3 on TAMs represents a promising area for further exploration, especially for the understanding of the interplay between TAMs and T cells in the TNBC immunosuppresive microenvironment.

Given the higher levels of secreted Gal-3 in TNBC and the aim to

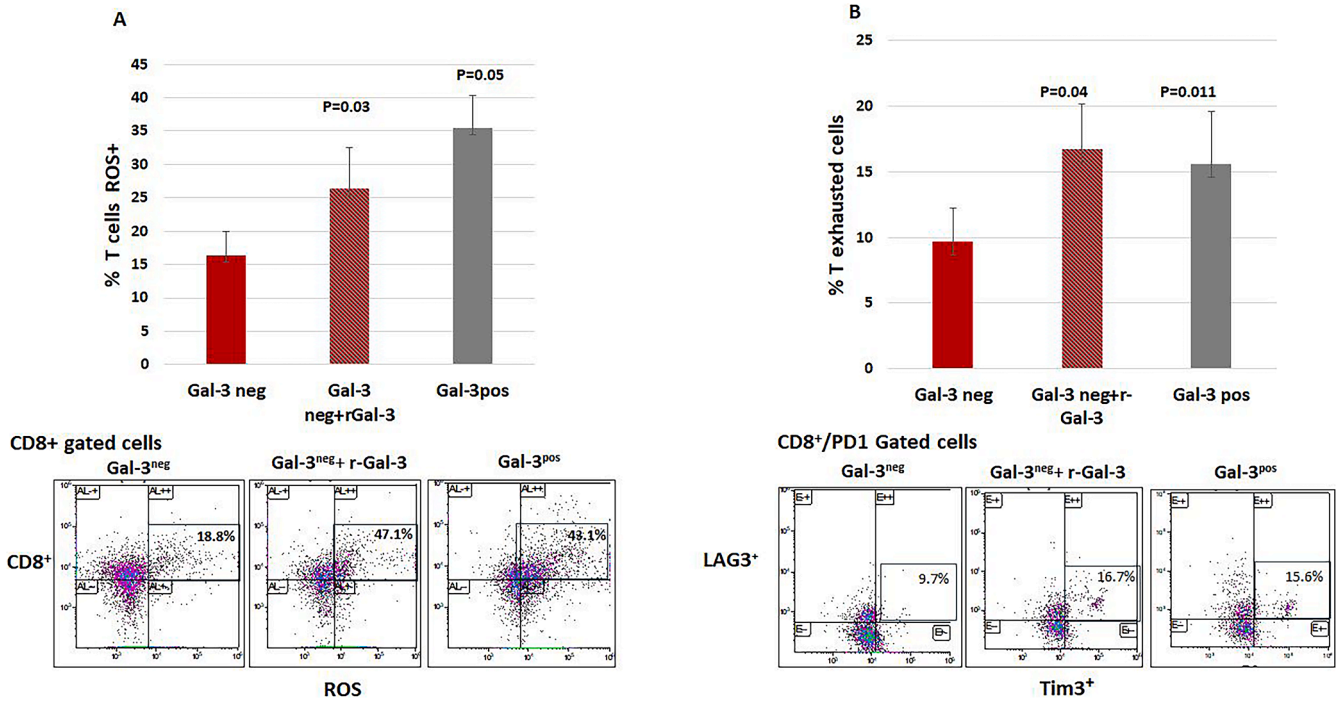

Figure 6. The effect of Gal-3 on intracellular reactive oxygen species (ROS) and T exhausted cells.
A. Flow cytometry analysis of the percentage of intracellular ROS in gated CD8+ cells from co-cultures of PBMCs with Gal-3^{neg} ± *r*-Gal-3 or with Gal-3^{pos} clones. The mean±SE was calculated from seven experiments using PBMCs from different healthy women. The statistical significance was calculated by ANOVA. Below, a representative flow cytometry analysis of gated CD8+/ROS+ cells. **B.** Flow cytometry analysis of the percentage of CD8/PD1 gated cells positive for Tim-3 and Lag-3 (T exhausted cells) in the three groups after 5 days incubation. Mean±SE of 14 experiments. The statistical significance was calculated by ANOVA.

reveal the mechanism of Gal-3 immunosuppression induction, we used RNA-sequencing to compare PBMCs of women with metastatic TNBC to those of healthy women. After deconvolution, we observed significant lower expression of genes involved in oxidative phosphorylation, specifically in T cells of TNBC patients. In agreement, T cells isolated from the peripheral blood of women with TNBC showed downregulation of *SLC25A6, MDH2, GPI* and *GOT2,* as evaluated by RT-PCR. Only the SUPV3L1 gene showed slightly greater expression in T cells of women with TNBC than in healthy women. This latter result could be related to differences between the women in their levels of Gal-3. In our in vitro model, we further evaluated the expression of those five genes by RT-PCR. The expression was lower of *SLC25A6, MDH2, SUPV3L1, GPI* and *GOT2* in isolated T cells co-cultured with Gal-3^{pos} TNBC cells, compared to T cells co-cultured with Gal-3^{neg} TNBC cells. Previously, Gal-3 was shown to be involved in mitochondrial metabolism in tumor cells, by improving the metabolic reprogramming of tumors, which enabled adaptation to the stressed microenvironment caused by oxygen and nutrient deprivation [42,43]. In addition to their involvement in mitochondrial functions, SLC25A6 and MDH2 expression are associated with the proliferation of activated T cells [8,44]. SUPV3L1 downregulation was found to induce cell apoptosis [45]. GPI expression was linked to the initiation of T cell activation through the antigen receptor complex, as well as the regulation of ongoing responses supported by enduring antigen exposure [46]. All TNBC patients in this study were Stage 4, and their plasma and PBMC samples were collected prior to treatment. Plasma Gal-3 levels were evaluated in these patients, though due to the small sample size ($n = 7$), no statistical correlation was drawn between plasma Gal-3 levels and other molecular data such as RNA sequencing or T cell gene expression.

In people with cancer, T-cells are continuously stimulated by exposure to tumor antigens, which eventually lead to an exhausted differentiated state [47]. A central feature of T cell exhaustion relates to an impaired mitochondrial state, which results in increased ROS production [48,49]. CD8+ *T* cells with depolarized mitochondria were found to be non-proliferative and hypofunctional, while expressing higher levels of exhaustion markers Tim-2, Lag-3 and PD1 [50]. In this study we observed significantly lesser lymphocyte proliferation in the presence of Gal-3. Gal-3 also induced a decrease in the expression of genes involved in oxidative phosphorylation in T cells, in correlation with significantly increased ROS production. An increase in intracellular ROS by CD8 cells resulted in a significant increase in T exhausted cells, only after a long exposure to Gal-3.

To conclude, we revealed a novel Gal-3 suppresor mechanism that affected both CD4 and CD8 cells. We demonstrated that Gal-3 secreted by TNBC cells induced an increase in tumor infiltrating T-reg. Additionally, Gal-3 led to imbalances in T cell mitochondrial function, which resulted in a gradual increase in T-exhausted cells, with loss of an immune anti-tumor response.

Understanding the effects of TNBC-secreted Gal-3 on T cell functions provides critical insights into the variable clinical responses to immunotherapy observed in women with TNBC. This understanding could contribute significantly to the development of novel therapeutic strategies aimed at improving TNBC treatment outcomes. Several studies have explored potential treatments targeting cancers with elevated Gal-3 levels. For instance, synthesized multivalent glycopolymer inhibitors, which effectively target both extracellular and intracellular Gal-3, have demonstrated promising results, including inhibition of cancer cell spread and modulation of tumor immune evasion [51]. In our study, we observed a decrease in regulatory Tregs in Gal-3-positive co-cultures treated with a Gal-3 antibody, further highlighting Gal-3 as a compelling target for immunotherapy.

We believe our study provides a broader framework to explore combination strategies, such as pairing biomaterial-based delivery systems with immunotherapy to enhance efficacy.

CRediT authorship contribution statement

Annat Raiter: Writing – review & editing, Writing – original draft, Supervision, Investigation, Funding acquisition, Conceptualization. **Yael Barhum:** Writing – original draft, Methodology, Investigation. **Julia Lipovetsky:** Methodology, Investigation, Data curation. **Chen Menachem:** Methodology, Formal analysis, Data curation. **Sharona Elgavish:** Writing – original draft, Methodology, Formal analysis, Data curation. **Shmuel Ruppo:** Methodology, Formal analysis, Data curation. **Yehudit Birger:** Supervision, Funding acquisition. **Shai Izraeli:** Supervision, Funding acquisition. **Orna Steinberg-Shemer:** Writing – review & editing, Supervision, Funding acquisition. **Rinat Yerushalmi:** Writing – review & editing, Funding acquisition, Conceptualization.

Declaration of competing interest

The authors declare that they have no known competing financial interests or personal relationships that could have appeared to influence the work reported in this paper.

Funding

The research was partially supported by Roche Breast Cancer Grant (2022-2023, Rinat Yerushalmi, Annat raiter) and by the Israel Innovation Authority, as part of the CRISPR-IL consortium (Yehudit Birger, Shai Izraeli, Orna Steinberg-Shemer).

Data availability statement

The data presented in the study is available in the article and on reasonable request from the corresponding author.

Supplementary materials

Supplementary material associated with this article can be found, in the online version, at doi:10.1016/j.neo.2024.101117.

References

[1] X. Zhang, Molecular classification of breast cancer, Arch. Pathol. Lab. Med. 147 (2022), 46-5.
[2] X. Li X, J. Yang, L. Peng, A.A. Sahin, L. Huo, K.C. Ward, R. O'Regan, M.A. Torres, J. L. Meisel, Triple-negative breast cancer has worse overall survival and cause-specific survival than non-triple-negative breast cancer, Breast. Cancer Res. Treat. 161 (2017) 279–287.
[3] S. Zhu, Y. Wu, B. Song, Y. Ming, Y. Yan, Q. Mei, K. Wu, Recent advances in targeted strategies for triple-negative breast cancer, J. Hematol. Oncol. 16 (2023) 100, https://doi.org/10.1186/s13045-023-01497-3.
[4] R.A. Leon-Ferre, M.P. Goetz, Advances in systemic therapies for triple negative breast cancer, BMJ 381 (2023) e071674.
[5] M.R. Girotti, M. Salatino, T. Dalotto-Moreno, G.A. Rabinovich, Sweetening the hallmarks of cancer: galectins as multifunctional mediators of tumor progression, J. Exp. Med. 217 (2) (2020) e20182041.
[6] E. Capone, S. Iacobelli, G. Sala, Role of galectin 3 binding protein in cancer progression: a potential novel therapeutic target, J. Transl. Med. 19 (2021) 405, https://doi.org/10.1186/s12967-021-03085-w.
[7] A. Romero, H.J. Gabius, Galectin-3: is this member of a large family of multifunctional lectins (already) a therapeutic target? Expert. Opin. Ther. Targets. 23 (10) (2019) 819–828, https://doi.org/10.1080/14728222.2019.1675638.
[8] P.P. Ruvolo, Galectin 3 as a guardian of the tumor microenvironment, Biochimica et Biophysica Acta (BBA) - Molecular Cell Research 1863 (3) (2016) 427–437, https://doi.org/10.1016/j.bbamcr.2015.08.008.
[9] Y. Guo, R. Shen, L. Yu, X. Zheng, R. Cui, Y. Song, D. Wang, Roles of galectin3 in the tumor microenvironment and tumor metabolism, Oncol. Rep. 44 (2020) 1799–1809.
[10] R. Dong, M. Zhang, Q. Hu, S. Zheng, A. Soh, Y. Zheng, H. Yuan, Galectin-3 as a novel biomarker for disease diagnosis and a target for therapy, Int. J. Mol. Med. 41 (2) (2018) 599–614, https://doi.org/10.3892/ijmm.2017.3311.
[11] A. Sedlář, M. Trávníčková, P. Bojarová, M. Vlachová, K. Slámová, V. Křen, L. Bačáková, Interaction between Galectin-3 and Integrins Mediates Cell-Matrix Adhesion in Endothelial Cells and Mesenchymal Stem Cells, Int. J. Mol. Sci. 22 (10) (2021) 5144, https://doi.org/10.3390/ijms22105144.
[12] H. Chen, A. Fermin, S. Vardhana, I. Weng, K.F.R. Lo, E. Chang, E. Maverakis, R. Yang, D.K. Hsu, M.L. Dustin, F. Liu, Galectin-3 negatively regulates TCR-

mediated CD4+ T-cell activation at the immunological synapse, Proc. Natl. Acad. Sci. U.S.A. 106 (34) (2009) 14496–14501, https://doi.org/10.1073/pnas.0903497106.
[13] A. Funkhouser, H. Shuster, J.C. Martin, W.J. Edenfield, A.V. Blenda, Pattern Analysis of Serum Galectins-1, -3, and -9 in Breast Cancer, Cancers. (Basel) 15 (15) (2023) 3809, https://doi.org/10.3390/cancers15153809.
[14] A. Raiter, O. Zlotnik, J. Lipovetsky, S. Mugami, S. Dar, I. Lubin, E. Sharon, C. J. Cohen, R. Yerushalmi, A novel role for an old target: CD45 for breast cancer immunotherapy, Oncoimmunology. 10 (1) (2021) 1929725, https://doi.org/10.1080/2162402X.2021.1929725.
[15] A. Raiter, J. Lipovetsky, A. Stenbac, I. Lubin, R. Yerushalmi, TNBC-derived Gal3BP/Gal3 complex induces immunosuppression through CD45 receptor, Oncoimmunology. 12 (1) (2023) 2246322, https://doi.org/10.1080/2162402X.2023.2246322.
[16] Y. Yamaguchi, J. Ohno, A. Sato, K. Hirofumi, T. Fukushima, Mesenchymal stem cell spheroids exhibit enhanced in-vitro and in-vivo osteoregenerative potential, BMC. Biotechnol. 14 (105) (2014), https://doi.org/10.1186/s12896-014-0105-9.
[17] M. Marcel, Cutadapt removes adapter sequences from high-throughput sequencing reads, EMBnet. J. 17 (1) (2011) 10–12, https://doi.org/10.14806/ej.17.1.200.
[18] D. Kim, G. Pertea, C. Trapnell, H. Pimentel, R. Kelley, S.L. Salzberg, TopHat2: accurate alignment of transcriptomes in the presence of insertions, deletions and gene fusions, Genome Biol. 14 (2013) R36.
[19] S. Anders, T.P. Pyl, W. Huber, HTSeq — A Python framework to work with high-throughput sequencing data, Bioinformatics. 31 (2) (2015) 166–169, https://doi.org/10.1093/bioinformatics/btu638.
[20] M.I. Love, W. Huber, S. Anders, Moderated estimation of fold change and dispersion for RNA-seq data with DESeq2, Genome Biol. 15 (2014) 550, https://doi.org/10.1186/s13059-014-0550-8.
[21] H. Jin, Y.W. Wan, Z. Liu, Comprehensive evaluation of RNA-seq quantification methods for linearity, BMC. Bioinformatics. 18 (Suppl 4) (2017) 117, https://doi.org/10.1186/s12859-017-1526-y.
[22] A.M. Newman, C.B. Steen, C.L. Liu, A.J. Gentles, A.A. Chaidhuri, F. Scherer, M. S. Khoudadoust, M.S. Esfahani, B.A. Luca, D. Steiner, M. Diehn, A.A. Alizadeh, Determining cell type abundance and expression from bulk tissues with digital cytometry, Nat. Biotechnol. 37 (2019) 773–782, https://doi.org/10.1038/s41587-019-0114-2.
[23] G. Monaco, B. Lee, W. Xu, S. Mustafah, Y.Y. Hwang, C. Carré, N. Burdin, L. Visan, M. Ceccarelli, M. Poidinger, A. Zippelius, J. Pedro de Magalhães, A. Larbi, RNA-Seq Signatures Normalized by mRNA Abundance Allow Absolute Deconvolution of Human Immune Cell Types, Cell Rep. 26 (6) (2019) 1627–1640, https://doi.org/10.1016/j.celrep.2019.01.041, e7.
[24] H.D. Li, C.X. Lin, J. Zheng, GTFtools: a software package for analyzing various features of gene models, Bioinformatics. 38 (20) (2022) 4806–4808, https://doi.org/10.1093/bioinformatics/btac561.
[25] M.E. Ritchie, B. Phipson, D. Wu, Y. Hu, C.W. Law, W. Shi, G.K. Smyth, Limma powers differential expression analyses for RNA-sequencing and microarray studies, Nucleic. Acids. Res. 43 (7) (2015) e47, https://doi.org/10.1093/nar/gkv007.
[26] A. Subramanian, P. Tamayo, V.K. Mootha, S. Mukherjee, B.L. Ebert, M.A. Gillette, A. Paulovich, S.L. Pomeroy, T.R. Golub, E.S. Lander, J.P. Mesirov, Gene set enrichment analysis: a knowledge-based approach for interpreting genome-wide expression profiles, Proc Natl Acad Sci USA 102 (2005) 15545–15550, https://doi.org/10.1073/pnas.0506580102.
[27] A. Hayashi A, S. Ruppo, E.E. Heilbrun, C. Mazzoni, S. Adar, M. Yassour, A. A. Rmaileh, S. Ydgeni, A web server to identify gene set enrichments in tumor samples, Comput. Struct. Biotechnol. J. 21 (2023) 5531–5537, https://doi.org/10.1016/j.csbj.2023.10.053.
[28] C.M. Capelle, S. Ciré, W. Ammerlaan, M. Konstantinou, R. Balling, F. Betsou, A. Cosma, M. Ollert, F.Q. Hefeng, Standard Peripheral Blood Mononuclear Cell Cryopreservation Selectively Decreases Detection of Nine Clinically Relevant T Cell Markers, Immunohorizons. 5 (8) (2021) 711–720, https://doi.org/10.4049/immunohorizons.2100049.
[29] Z. Lyu, Y. Chen, X. Guo, F. Zhou, Z. Yan, J. Xing, J. An, H. Zhang, Genetic variants in glucose-6-phosphate isomerase gene as prognosis predictors in hepatocellular carcinoma, Clin. Res. Hepatol. Gastroenterol. 40 (6) (2016) 698–704, https://doi.org/10.1016/j.clinre.2016.05.001.
[30] J.S. Bhatti, G.K.P. Bhatti, H. Reddy, Mitochondrial dysfunction and oxidative stress in metabolic disorders — A step towards mitochondria based therapeutic strategies, Biochimica et Biophysica Acta (BBA) - Molecular Basis of Disease 1863 (5) (2017) 1066–1077.
[31] J. Ježek, K.F. Cooper, R. Strich R, Reactive oxygen species and mitochondrial dynamics: the Yin and Yang of mitochondrial dysfunction and cancer progression, Antioxidants 7 (1) (2018) 13, https://doi.org/10.3390/antiox7010013.
[32] A. Marra, D. Trapani, G. Viale, C. Criscitiello, G. Curigliano, Practical classification of triple-negative breast cancer: intratumoral heterogeneity, mechanisms of drug resistance, and novel therapies, NPJ. Breast. Cancer 6 (2020) 54, https://doi.org/10.1038/s41523-020-00197-2.
[33] K. Asleh, N. Riaz, T.O. Nielsen, Heterogeneity of triple negative breast cancer: current advances in subtyping and treatment implications, J. Exp. Clin. Cancer Res. 41 (2022) 265, https://doi.org/10.1186/s13046-022-02476-1.
[34] A. Shafiq, J. Moore, A. Suleman, S. Faiz, O. Farooq, A. Arshad, M. Tehseen, A. Zafar, S.H. Ali, N.U. Din, A. Loya, N. Siddiqui, F.K. Rehman, Elevated Soluble Galectin-3 as a Marker of Chemotherapy Efficacy in Breast Cancer Patients: a Prospective Study, Int. J. Breast. Cancer 14 (2020) 4824813, https://doi.org/10.1155/2020/4824813.
[35] H. Zhang, M. Luo, X. Liang, D. Wang, X. Gu, C. Duan, H. Gu, G. Chen, X. Zhao, Z. Zhao, C. Liu, Galectin-3 as a marker and potential therapeutic target in breast cancer, PLoS. One 9 (9) (2014) e103482.
[36] D. Niang, S. Ka, J. Hendricks, D. Diouf, F. Gaba, A. Diouf, M. Diop, M. Mbow, B. Faye, R. Diallo, M. Niang, A. Deme, B. Mbengu, A. Dieye, Profile of Plasma Galectin-3 Concentrations, Inflammatory Cytokines Levels and Lymphocytes Status in Breast Cancer under Chemotherapy, Open. J. Immunol. 12 (2022) 1–14, https://doi.org/10.4236/oji.2022.121001.
[37] B.K. Moon, Y.J. Lee, P. Battle, J.M. Jessup, A. Raz, H.R. Choi Kim, Galectin-3 Protects Human Breast Carcinoma Cells against Nitric Oxide-Induced Apoptosis: implication of Galectin-3 Function during Metastasis, Am. J. Pathol. 159 (3) (2001) 1055–1060, https://doi.org/10.1016/S0002-9440(10)61780-4.
[38] Y. Honjo, P. Nangia-Makker, H. Inohara, A. Raz, Down-regulation of galectin-3 suppresses tumorigenicity of human breast carcinoma cells, Clin Cancer Re 7 (2001) 661–668.
[39] P. Nangia-Makker, V. Balan, A. Raz, Regulation of Tumor Progression by Extracellular Galectin-3, Cancer Microenvironment 1 (2008) 43–51, https://doi.org/10.1007/s12307-008-0003-6.
[40] R.C. Gilson, S.D. Gunasinghe, L. Johannes, K. Gaus, Galectin-3 modulation of T-cell activation: mechanisms of membrane remodeling, Prog. Lipid Res. 76 (2019) 101010, https://doi.org/10.1016/j.plipres.2019.101010.
[41] Y. Zhang, S. Cheng, M. Zhang, L. Zhen, D. Pang, Q. Zhang Q, et al., High-Infiltration of Tumor-Associated Macrophages Predicts Unfavorable Clinical Outcome for Node-Negative Breast Cancer, PLoS. One 8 (9) (2013) e76147, https://doi.org/10.1371/journal.pone.0076147.
[42] R. Lakshminarayan, C. Wunder, U. Becken, M.T. Howes, C. Benzing, S. Arumugam, S. Sales, N. Ariotti, V. Chambon, C. Lamaze, D. Loew, A. Shevchenko, K. Gaus, R. G. Parton, L. Johannes, Galectin-3 drives glycosphingolipid-dependent biogenesis of clathrin-independent carriers, Nat. Cell Biol. 16 (2014) 592–603.
[43] Y.S. Li, X.T. Li, L.G. Yu, L. Wang, Z.Y. Shi, X.L. Guo, Roles of galectin-3 in metabolic disorders and tumor cell metabolism, Int. J. Biol. Macromol. 142 (2020) 463–473.
[44] A.R. Liu, Y.N. Liu, S.X. Shen, L.R. Yan, Z. Lv, H.X. Ding, A. Wang, Y. Yuan, Q. Xu, Comprehensive Analysis and Validation of Solute Carrier Family 25 (SLC25) and Its Correlation with Immune Infiltration in Pan-Cancer, Biomed. Res. Int. 2022 (2022) 4009354, https://doi.org/10.1155/2022/4009354.
[45] T. Eleftheriadis, G. Pissas, G. Antoniadi, V. Liakopoulos, I. Stefanidis, Malate dehydrogenase-2 inhibitor LW6 promotes metabolic adaptations and reduces proliferation and apoptosis in activated human T-cells, Exp. Ther. Med. 10 (5) (2015) 1959–1966, https://doi.org/10.3892/etm.2015.2763.
[46] E. Paul, M. Kielbasinski, J.M. Sedivy, C. Murga-Zamalloa, H. Khanna, J.E. Klysik, Widespread expression of the Supv3L1 mitochondrial RNA helicase in the mouse, Transgenic Res. 19 (4) (2010) 691–701, https://doi.org/10.1007/s11248-009-9346-0.
[47] M.D. Marmor, M. Julius, The function of GPI-anchored proteins in T cell development, activation and regulation of homeostasis, J. Biol. Regul. Homeost. Agents 14 (2) (2000) 99–115.
[48] Z. Gao, Y. Feng, J. Xu, J. Liang, T-cell exhaustion in immune-mediated inflammatory diseases: new implications for immunotherapy, Front. Immunol. 13 (2022) 977394, https://doi.org/10.3389/fimmu.2022.977394.
[49] N.E. Scharping, D.B. Rivadeneira, A.V. Menk, P.D.A. Vignali, B.R. Ford, N. L. Rittenhouse, R. Peralta, Y. Wang, Y. Wang, K. DePeaux, A.C. Poholek, G. M. Delgoffe, Mitochondrial stress induced by continuous stimulation under hypoxia rapidly drives T cell exhaustion, Nat. Immunol. 22 (2021) 205–215.
[50] F.C. Richter, M. Saliutina, A.N. Hegazy, A. Bergthaler, Take my breath away—Mitochondrial dysfunction drives CD8+ T cell exhaustion, Genes. Immun. 25 (2024) 4–6, https://doi.org/10.1038/s41435-023-00233-8.
[51] W. Zhu, Y. Li, M. Han, J. Jiang, Regulatory Mechanisms and Reversal of CD8+T Cell Exhaustion: a Literature Review, Biology. (Basel) 12 (4) (2023) 541, https://doi.org/10.3390/biology12040541.